von Neumann entropy spectra and entangled excitations in spin-orbital models

Wen-Long You,[1,2] Andrzej M. Oleś,[1,3] and Peter Horsch[1]
[1]*Max-Planck-Institut für Festkörperforschung, Heisenbergstrasse 1, D-70569 Stuttgart, Germany*
[2]*School of Physical Science and Technology, Soochow University, Suzhou, Jiangsu 215006, People's Republic of China*
[3]*Marian Smoluchowski Institute of Physics, Jagellonian University, Reymonta 4, PL-30059 Kraków, Poland*
(Received 30 March 2012; published 10 September 2012)

We consider the low-energy excitations of one-dimensional spin-orbital models which consist of spin waves, orbital waves, and joint spin-orbital excitations. Among the latter we identify strongly entangled spin-orbital bound states and spin-orbital quasiparticle states which appear as peaks in the von Neumann entropy spectral function introduced in this work. We present the scaling of the von Neumann entropy with system size and find a qualitatively different behavior for the bound state and the quasiparticle—the strong entanglement of these states is manifested by a universal logarithmic scaling of the von Neumann entropy with system size, while the entropy saturates for other spin-orbital excitations. We suggest that spin-orbital entanglement can be experimentally explored by the measurement of the dynamical spin-orbital correlations using resonant inelastic x-ray scattering, where strong spin-orbit coupling associated with the core hole plays a role.

DOI: 10.1103/PhysRevB.86.094412 PACS number(s): 75.10.Jm, 03.65.Ud, 03.67.Mn, 75.25.Dk

I. INTRODUCTION

The spin-orbital interplay is one of the important topics in the theory of strongly correlated electrons.[1,2] In many cases, the intertwined spin-orbital interaction is decoupled by mean field approximation, and the spin and orbital dynamics are independent of each other. Thus a spin-only Heisenberg model can be derived by averaging over the orbital state, which successfully explains magnetism and optical excitations in some materials, for instance in $LaMnO_3$.[3] But in others, especially in t_{2g} systems,[4] the orbital degeneracy plays an indispensable role in understanding the low-energy properties in the Mott insulators of transition metal oxides, such as $LaTiO_3$,[5] $LaVO_3$, and YVO_3,[6] and also in recently discussed RbO_2.[7] Of high interest are systems with strong spin-orbit coupling which leads to locally entangled states,[8] and entanglement on the superexchange bonds in $K_3Cu_2F_7$.[9] For such systems, the mean-field-type approximation and the decoupling of composite spin-orbital correlations fail and generate uncontrolled errors, even when the orbitals are polarized.[10] The strong spin-orbital fluctuations on the exchange bonds will induce the violation of the Goodenough-Kanamori rules,[11] or measurable consequences in transition metal oxides at finite temperature.[12] Furthermore, the different flavors may form exotic composite spin-orbital excitations.

Whereas the study of elementary spin excitations, i.e., the spin waves, is experimental routine, the exploration of orbitons proved much more difficult experimentally[13–15] than theoretically.[16–22] Only recently clear experimental signatures of orbitons have been found in the quasi-one-dimensional Mott insulator Sr_2CuO_3.[2] The observation of pronounced momentum dependence of their energy reflects their nature as propagating excitations, and distinguishes them from localized crystal-field excitations.[23] Coupled spin-orbital excitations that could shed light on the entanglement of the two distinct degrees of freedom, i.e., spin and orbital, have so far not been detected and explored in experiments as far as we are aware. The aim of this paper is to study a simple spin-orbital model[24–27] which is known to feature collective spin-orbital excitations,[28–30] and to explore what can be learned from such excitations concerning the entanglement of the different degrees of freedom. We also address the question of which type of spectroscopies might be useful to explore the entanglement of such excitations.

A paradigmatic model derived for a transition metal oxide system in the Mott-insulating limit is the one-dimensional (1D) spin-orbital Hamiltonian,[24,25] which reads

$$H = -J \sum_{\mathbf{i}} (\vec{S}_{\mathbf{i}} \cdot \vec{S}_{\mathbf{i}+1} + x)(\vec{T}_{\mathbf{i}} \cdot \vec{T}_{\mathbf{i}+1} + y), \qquad (1)$$

where $\vec{S}_{\mathbf{i}}$ and $\vec{T}_{\mathbf{i}}$ are spin-1/2 and pseudospin-1/2 operators representing the spin and orbital degrees of freedom located at site $\mathbf{i}$, respectively, and we set below $J = 1$. It is proposed that ultracold fermions in zigzag optical lattices can reproduce an effective spin-orbital model.[31] For general $\{x, y\}$, the model (1) has an SU(2)⊗SU(2) symmetry. An additional $\mathbf{Z}_2$ bisymmetry occurs by interchanging spin and orbital operators when $x = y$. In the case of $x = y = \frac{1}{4}$, Hamiltonian (1) reduces to a SU(4) symmetric model, which is exactly soluble by the Bethe ansatz.[32,33] There are three Goldstone modes corresponding to separate spin and orbital excitation, as well as composite spin-orbital excitations in the case of $J < 0$, in contrast to a quadratic dependence of the energy upon the momentum in the long-wave limit for $J > 0$. The spectra of elementary excitations are commonly not analytically soluble away from the SU(4) point. We will, however, show that the low-energy excitations can be analytically obtained in some specific phases in the case when $J > 0$, and this offers a platform to study the spin-orbital entanglement. In this paper, we go beyond the ideas developed for spin systems.[34] We demonstrate that spin-orbital entanglement entropy clearly distinguishes weakly correlated spin-orbital excitations from bound states and resonances by its magnitude and distinct scaling behavior. We propose how to connect the entanglement entropy with experimentally observable quantities of recently developed spectroscopies.

Currently, concepts from quantum information theory are being studied with the aim to explore many-body theory from another perspective and vice versa. A particularly fruitful direction is using quantum entanglement to shed light on exotic

quantum phases.[35,36] Entanglement entropy even distinguishes phases in the absence of conventional order parameters.[37] In general, a many-body quantum system is subdivided into A and B parts, and the entanglement entropy is the von Neumann entropy (vNE), $\mathcal{S}_{\rm vN} = -{\rm Tr}\{\rho_A \log_2 \rho_A\}$, where $\rho_A = {\rm Tr}_B\{\rho\}$ is the reduced density matrix of the subspace A and ρ is the full density matrix. The vNE is bounded, $\mathcal{S}_{\rm vN} \leqslant \log_2 {\rm dim}\rho_A$, and easy to calculate. Experimental determination appears harder, yet there are proposals involving transport measurements in quantum point contacts.[38]

Interestingly the vNE scales proportionally to the boundary of the subregion obtained by the spatial partitioning.[39] The dependence of the boundary or area law can be traced back to the study of black hole physics[40] and was extensively exploited for 1D spin chains.[41] If the block A is of length l in a system of length L with periodic boundary condition, the vNE of gapped ground states is bounded as $\mathcal{S}_l = \mathcal{O}(1)$, while a logarithmic scaling $\mathcal{S}_l = c \log_2 l + \mathcal{O}(1)$ $(L \gg l \gg 1)$ has been proven to be universal property of the gapless phases in critical systems by the underlying conformal field theory.[42] A violation of the area law is expected for the low-lying excited states of critical chains.[43] In a composite system containing spin and orbital operators, the decomposition of different flavors retains the real-space symmetries. To date, measurements of the vNE for subdivision of degrees of freedom other than in spatial segmentation have not been fully explored.[44]

The paper is organized as follows. First, in Sec. II, we present the phase diagram of the 1D spin-orbital model (1), including the exact bound on the ground state energy of the ferro-ferro state considered here. We also analyze the elementary excitation spectrum of this phase and introduce the bound state (BS) and spin-orbital quasiparticle (SOQ) state which occur in the spectra. In Sec. III we present the vNE spectra and the scaling behavior of the SOQ state. Next we consider possible experimental observation of the dynamical spin-orbital correlations using resonant inelastic x-ray scattering (RIXS) in Sec. IV. The paper is summarized in Sec. V.

II. PHASE DIAGRAM AND EXCITATIONS

A quantum phase transition (QPT) is identified as a point of nonanalyticity of the ground state and associated expectation values in the thermodynamic limit. To shed light on the phase boundaries of the 1D spin-orbital model,[24,25] we first consider two sites,

$$H_{12} = -\tfrac{1}{4}\big(\vec{S}_{12}^2 - \vec{S}_1^2 - \vec{S}_2^2 + 2x\big)\big(T_{12}^2 - \vec{T}_1^2 - \vec{T}_2^2 + 2y\big), \quad (2)$$

where $\vec{S}_{12} = \vec{S}_1 + \vec{S}_2$ and $\vec{T}_{12} = \vec{T}_1 + \vec{T}_2$. A pair of spins (orbitals) can form either a singlet with $S_{12} = 0$ $(T_{12} = 0)$ or a triplet with $S_{12} = 1$ $(T_{12} = 1)$, and various combinations of quantum numbers correspond to different phases shown in Fig. 1. In phase I, the state with $S_{12} = 1 = T_{12}$ has the lowest energy, and thus the energy per bond is $e_B^I \geqslant e_{xy} = -(x + 1/4)(y + 1/4)$. For a larger system with L bonds, we have $E_0^I(H) \geqslant Le_{xy}$. On the other hand, taking a ferro-ferro state $|0\rangle$ as a variational state, $E_0^I(H) \leqslant Le_{xy}$. Therefore, the energy of phase I is exactly $E_0^I(H) = Le_{xy}$ and the ferro-ferro state is the corresponding ground state in the thermodynamic limit.

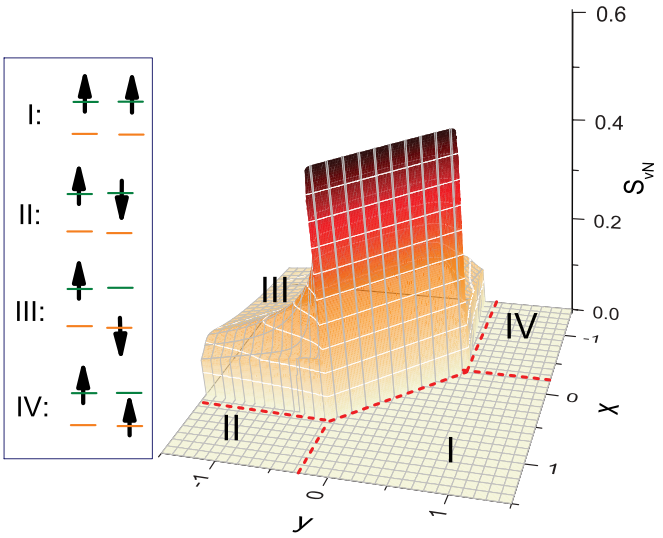

FIG. 1. (Color online) Spin-orbital entanglement entropy $\mathcal{S}_{\rm vN}$ in the ground state of the spin-orbital model (1) as a function of x and y, obtained for system size $L = 8$. The dashed (red) lines mark the critical lines determined by the fidelity susceptibility (see text). The two-site configurations in phases I-IV are shown on the left. The two orbitals per site are degenerate (their splitting is shown only for clarity of presentation).

Without prior knowledge of order parameter, various characterizations from the perspective of quantum information theory can be used to identify phase boundaries. One often used tool is the vNE.[45] Tracing orbital degrees of freedom, we obtained the spin-orbital vNE $\mathcal{S}_{\rm vN}$ for the ground state of $L = 8$ chain in the Hilbert subspace of $S_z = T_z = 0$.[45] However, here we find that the vNE of the ground state does not distinguish phase I from phase II or IV—all three phases having $\mathcal{S}_{\rm vN} = 0$ (see Fig. 1). Therefore we use the quantum fidelity to quantify the phase diagram.[46] The fidelity defined as follows, $\mathcal{F}(\lambda,\delta\lambda) = |\langle\Psi_0(\lambda)|\Psi_0(\lambda + \delta\lambda)\rangle|$, is taken along a certain path $\{x(\lambda), y(\lambda)\}$ and reveals all phase boundaries. The fidelity susceptibility, $\chi_{\rm F} \equiv -(2\ln\mathcal{F})/(\delta\lambda)^2|_{\delta\lambda\to 0}$, exhibits a peak at the critical point, and can be treated as a versatile order parameter in distinguishing ground states.[47] It signals the phase boundaries shown in Fig. 1. Remarkably, the phase diagram found from the fidelity susceptibility for larger systems is the same as the one for $L = 2$.

In phase I of Fig. 1, with boundaries given by $x + y = \frac{1}{2}$, $x = -\frac{1}{4}$ and $y = -\frac{1}{4}$, the spins and orbitals are fully polarized, and the ferro-ferro ground state $|0\rangle$ is disentangled, i.e., can be factorized into spin and orbital sectors. It is now interesting to ask whether: (i) the vanishing spin-orbital entanglement in the ground state implies a suppression of joint spin-orbital quantum fluctuations, and (ii) collective spin-orbital excitations can form. Using the equation of motion method one finds spin (magnon) excitations with dispersion

$$\omega_s(Q) = \big(\tfrac{1}{4} + y\big)(1 - \cos Q), \quad (3)$$

and orbital (orbiton) excitations,[30]

$$\omega_t(Q) = \big(\tfrac{1}{4} + x\big)(1 - \cos Q). \quad (4)$$

The stability of the orbitons (magnons) implies that $x > -\frac{1}{4}$ ($y > -\frac{1}{4}$), and determines the QPT between phases I and II (IV), respectively, while the spin-orbital coupling only renormalizes the spectra.

For our purpose, it is straightforward to consider the propagation of a magnon-orbiton pair excitation along the ferro-ferro chain, by simultaneously exciting a single spin and a single orbital. The translation symmetry imposes that total momentum $Q = 2m\pi/L$ $(m = 0, \ldots, L-1)$ is conserved during scattering. The scattering of magnon and orbiton with initial (final) momenta $\{\frac{Q}{2} - q, \frac{Q}{2} + q\}$ ($\{\frac{Q}{2} - q', \frac{Q}{2} + q'\}$) and total momentum Q is represented by the Green's function,[48]

$$G(Q,\omega) = \frac{1}{L}\sum_{q,q'} \left\langle\!\left\langle S^{+}_{\frac{Q}{2}-q'} T^{+}_{\frac{Q}{2}+q'} \middle| S^{-}_{\frac{Q}{2}-q} T^{-}_{\frac{Q}{2}+q} \right\rangle\!\right\rangle, \tag{5}$$

for a combined spin ($S^{-}_{\frac{Q}{2}-q}$) and orbital ($T^{-}_{\frac{Q}{2}+q}$) excitation. The spin-orbital continuum is given by

$$\Omega(Q,q) = \omega_s\left(\frac{Q}{2} - q\right) + \omega_t\left(\frac{Q}{2} + q\right). \tag{6}$$

In the noninteracting case, the Green's function exhibits square-root singularities at the edges of the continuum.[49] Due to residual, attractive interactions spin-orbital BSs are shifted outside the continuum,[24,29,50] see Fig. 2(a). The collective mode is determined by

$$1 + \frac{1}{2\pi}\int_{-\pi}^{\pi} dq \frac{\left(\cos\frac{Q}{2} - \cos q\right)^2}{\omega_{\rm BS} - \Omega(Q,q)} = 0. \tag{7}$$

The analytic solution of this equation is tedious but straightforward. The collective BS with dispersion $\omega_{\rm BS}(Q)$ is well separated from the magnon-orbiton continuum [Fig. 2(a)] at large Q. In the long-wave limit the BS energy coincides with the Arovas-Auerbach line $x + y = \frac{1}{2}$,[51] which represents the boundary of the ferro-ferro phase (see Fig. 1), yet the BS remains undamped for $x + y > \frac{1}{2}$.

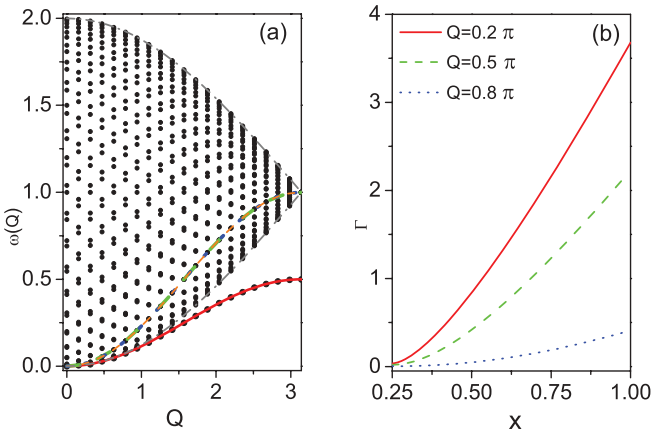

FIG. 2. (Color online) (a) Energy spectra of 40-site spin-orbital system at $x = y = 1/4$ as function of momentum Q. Dashed lines inside the spin-orbital continuum $\Omega(Q,q)$ denote the spin, orbital, and SOQ excitations, i.e., $\omega_s(Q)$, $\omega_t(Q)$ and $\omega_{\rm SOQ}(Q)$, respectively, that are all degenerate at the SU(4) point. The (red) solid line below the continuum corresponds to the spin-orbital BS. (b) The decay rate $\Gamma(Q)$ of the SOQ for different momenta $Q = 0.2, 0.6, 0.8\pi$ as a function of x, where $y = x$ and $L \to \infty$.

In addition, a collective mode of spin-orbital resonances,

$$|\Psi(Q)\rangle = \frac{1}{\sqrt{L}}\sum_{m,l} a_l(Q) e^{iQm} S^{-}_{m} T^{-}_{m+l} |0\rangle, \tag{8}$$

occurs inside the continuum. Here $0 \leqslant l \leqslant L-1$ denotes the distance between spin and orbital flips. Remarkably, the spin and orbital flips are glued together at the same site with $a_l(Q) = \delta_{l,0}$ at the SU(4) point.[30] This exact eigenstate of H Eq. (1) has been dubbed on-site BS. In order to distinguish it better from the typical collective BS's that lie below the continuum of spin-orbital excitations, and to account for the damping of this state away from the SU(4) point, we call it here the SOQ state. The SOQ has the dispersion

$$\omega_{\rm SOQ}(Q) = x + y - \tfrac{1}{2}\cos Q, \tag{9}$$

that is degenerate with both $\omega_s(Q)$ and $\omega_t(Q)$ at $x = y = \frac{1}{4}$, see Fig. 2(a). This is reminiscent of the degeneracy of the three Goldstone modes at the SU(4) point of the antiferromagnetic version of Hamiltonian (1), i.e., for $J = -1$.[32,33] Moving away from the SU(4) point, the SOQ decays due to residual interactions into magnon-orbiton pairs; simultaneously the mean separation ξ of spin and orbital excitations increases, i.e., $a_l(Q) \sim \exp(-l/\xi)$. This leads in the thermodynamic limit to a finite linewidth defined by $\Gamma = {\rm Im}\{G^{-1}(Q,\omega)\}$.[52] The decay rate of the SOQ increases with growing $x > \frac{1}{4}$ and also for decreasing momenta Q, as seen in Fig. 2(b).

III. VON NEUMANN ENTROPY SPECTRA

To investigate the degree of entanglement of spin-orbital excited states, we introduce the vNE spectral function in the Lehmann representation,

$$S_{\rm vN}(Q,\omega) = -\sum_{n} {\rm Tr}\left\{\rho_s^{(\mu)} \log_2 \rho_s^{(\mu)}\right\}\delta\{\omega - \omega_n(Q)\}, \tag{10}$$

where $(\mu) = (Q,\omega_n)$ denote momentum and excitation energy, and the spin density matrix, $\rho_s^{(\mu)} = {\rm Tr}_o|\Psi_n(Q)\rangle\langle\Psi_n(Q)|$, is obtained by tracing the orbital degrees of freedom. Our focus in the following are the elementary excitations of the system. Typically in solid state physics the elementary excitations are the excitations that characterize the system. Since these states are in the vicinity of the ground state they are also more easily accessible by experiment than highly excited states. Nevertheless, the definition in Eq. (10) holds for the full excitation spectrum, i.e., with a proper labeling μ for the excitations. For the elementary spin-orbital excitation the entanglement properties are encoded in the set of Schmidt coefficients $\{a_l(Q)\}$ in Eq. (8), and thus it follows from it that the diagonal form is

$$\rho_s^{(\mu)} = \sum_{q} |a_q|^2 S^{-}_{\frac{Q}{2}-q} |0\rangle\langle 0| S^{+}_{\frac{Q}{2}-q}, \tag{11}$$

where

$$a_q = \frac{1}{\sqrt{L}}\sum_{l} a_l(Q) e^{-i(\frac{Q}{2}-q)l}. \tag{12}$$

The eigenvalue spectrum of $\rho_s^{(\mu)}$ shows the basic entanglement feature between magnon and orbiton, and $\ln|a_q|^2$ has

been termed "entanglement spectrum" introduced by Li and Haldane.[35]

Let us consider first the symmetric case in Eq. (1), i.e., $x = y$. The Hilbert space can be divided into two subspaces characterized by the parity $P_{\rm ST}$ of the interchange of $S \leftrightarrow T$, which is either odd or even. Translation symmetry allows us to express the reduced density matrix ρ_s in a block-diagonal form, where each block corresponds to an irreducible representation labeled by total momentum Q and parity of exchange symmetry $P_{\rm ST}$. The vNE can be obtained by diagonalizing these blocks separately. In particular, the nondegenerate eigenstates with odd parity can be explicitly cast in the form $\frac{1}{\sqrt{2}}(S^-_{Q/2-q}T^-_{Q/2+q} - S^-_{Q/2+q}T^-_{Q/2-q})|0\rangle$. Consequently, the singletlike pair leads to $\mathcal{S}_{\rm vN} = 1$. For other spin-orbital eigenstates with $P_{\rm ST} = 1$, $\mathcal{S}_{\rm vN} \geqslant 1$, except the pure spin or pure orbital waves. Interestingly, we find that the parity is still conserved in subspace $Q = 0$ for $x \neq y$. The strongly entangled spin-orbital BSs are reflected by peaks in the von Neumann spectra $\mathcal{S}_{\rm vN}(Q,\omega)$, shown in Fig. 3. At the SU(4) point, the entanglement of the SOQ is larger than that of BS and is noted to be independent of momentum Q, as is displayed in Fig. 3(a). However, as momentum Q decreases, the SOQ peak in the center of the spectra gets broader in Fig. 3(b), implying a shorter lifetime.

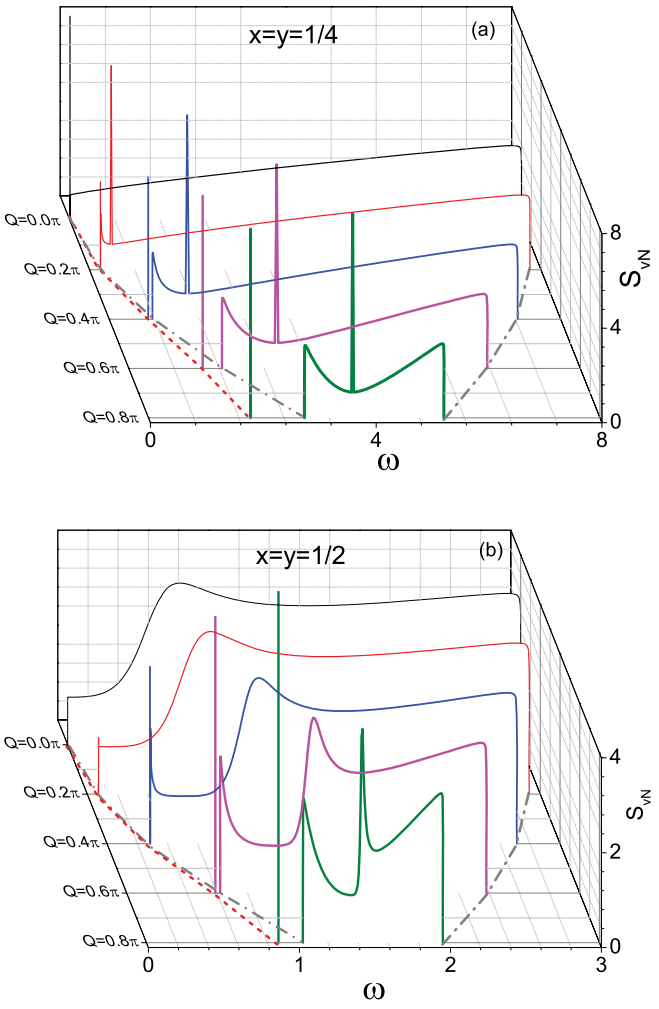

FIG. 3. (Color online) The vNE spectral function $S_{\rm vN}(Q,\omega)$ (10) as obtained for 400-site spin-orbital system in subspace $P_{\rm ST} = 1$ for different momenta Q, and for: (a) $x = y = 1/4$, (b) $x = y = 1/2$. Isolated vertical lines below the continuum indicate the BS, with dispersion given by the dashed (red) line. The SOQ in the center of spectra is undamped for case (a) while it is damped for case (b).

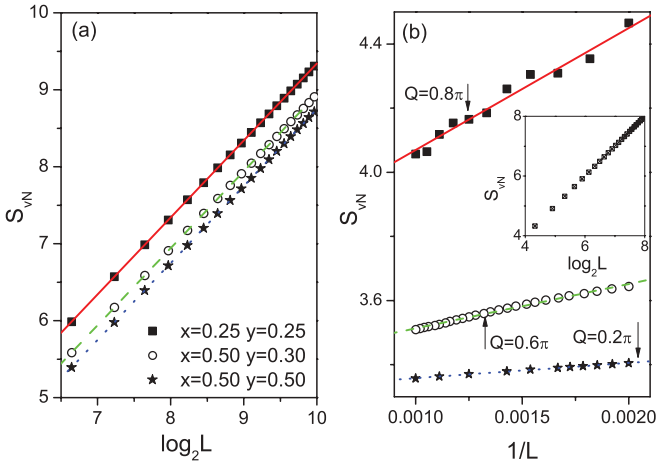

FIG. 4. (Color online) (a) Scaling behavior of entanglement entropy $\mathcal{S}_{\rm vN}$ of the spin-orbital BSs for $Q = 0.8\pi$. Lines represent logarithmic fits to Eq. (13), with $c_0 = -0.659, -1.059, -1.251$, respectively. (b) The scaling behavior of entanglement entropy of the SOQ for $x = y = 1/2$. Lines are fitted by $\mathcal{S}_{\rm vN} = c_1/L + c_0$, with c_0 $(c_1) = 3.69$ (380.5), 3.37 (138.4) and 3.31 (47.6) for $Q = 0.8\pi, 0.6\pi$ and 0.2π. The inset shows the logarithmic behavior of $\mathcal{S}_{\rm vN}$ for the SOQ with $Q = 0.8\pi$ and $x = y = 1/4$.

Inspection of the vNE spectra shows that the entanglement reaches a local maximum at the BSs. Finite size scaling of vNE of spin-orbital BSs reveals the asymptotic logarithmic scaling,

$$\mathcal{S}_{\rm vN} = \log_2 L + c_0, \tag{13}$$

shown in Fig. 4(a). The same logarithmic scaling is found for the SOQ at the SU(4) point $x = y = \frac{1}{4}$, as seen in the inset of Fig. 4(b). In this case, $a_q = L^{-1/2}$ and the equal weight for each q gives rise to the maximal entanglement, $\mathcal{S}_{\rm vN} = \log_2 L$. However, far away from the SU(4) point the scaling is entirely different and the entropy of the SOQ scales as a power law, $\mathcal{S}_{\rm vN} = c_1/L + c_0$, as seen in Fig. 4(b). This change of scaling from logarithmic to power law in $1/L$ is controlled by the correlation length ξ measuring the average distance of spin and orbital excitations in the SOQ wave function (8). From Eq. (8) and $a_l(Q) \sim \exp(-l/\xi)$ we obtain

$$|a_q|^2 \simeq \frac{2\pi\xi}{L\arctan(2\pi\xi)}\frac{1}{1+q^2\xi^2}. \tag{14}$$

The vNE can be cast in the asymptotic form by a little algebra,

$$\mathcal{S}_{\rm vN} \simeq \log_2\left\{\frac{L}{(1+\xi)}\right\}, \tag{15}$$

which yields $\log_2 L$ at $x = y = 1/4$ where $\xi = 0$. As ξ increases the correction to the vNE is $\propto -\log_2(1+\xi)$. Far away from the SU(4) point, the SOQ is damped and ξ becomes extensive, i.e., $\xi/L \approx \tilde{c}_0 - \tilde{c}_1/L$, and the vNE approaches a finite value with a correction $\propto 1/L$ as shown in Fig. 4(b). In other words for weak spin-orbital correlation, which

corresponds to large spin-orbital correlation length ξ, the entanglement entropy approaches a value of $O(1)$. We note that this dependence of the vNE in a spin-orbital system is distinct from the dependence of the vNE on the spin-correlation length in a pure spin system, as for example in the case of the quantum Ising model.[53] This close correspondence of the vNE of BSs and the correlation length ξ suggests to use the dynamic spin-orbital correlation function as a probe of spin-orbital entanglement and as a qualitative measure of the vNE spectra.

IV. RIXS SPECTRAL FUNCTIONS

Returning to transition metal oxides, one realizes that joint spin-orbital excitations are not created in the ferro-ferro ground state in photoemission spectroscopy because of spin conservation. On the contrary, the recently developed RIXS method[2,14,54–56] is in principle capable of measuring the spectral function of the coupled spin-orbital excitations at distance l,

$$A_l(Q,\omega) = \frac{1}{\pi}\lim_{\eta\to 0}\mathrm{Im}\langle 0|\Gamma_Q^{(l)\dagger}\frac{1}{\omega + E_0 - H - i\eta}\Gamma_Q^{(l)}|0\rangle. \tag{16}$$

Here

$$\Gamma_Q^{(0)} = \frac{1}{\sqrt{L}}\sum_j e^{iQj} S_j^- T_j^- \tag{17}$$

is the local excitation operator for an on-site spin-orbital excitation. We employ as well the even and odd parity operators,

$$\Gamma_Q^{(1_\pm)} = \frac{1}{\sqrt{2L}}\sum_j e^{iQj}(S_{j+1}^- \pm S_{j-1}^-)T_j^-, \tag{18}$$

to probe the nearest-neighbor spin-orbital excitations. In the RIXS process an electron with spin up is excited by the incoming x rays from a deep-lying core level into the valence shell. For the time of its existence the core hole generates a Coulomb potential and a strong spin-orbit coupling that allows for the nonconservation of spin. Next the hole is filled by an electron from the occupied valence band under the emission of an x ray. This RIXS process creates a joint spin-valence excitation with momentum Q_{in}-Q_{out} and energy ω_{in}-ω_{out}, which can unveil the spectral function of the spin-orbital excitation.

The on-site spectral function $A_0(Q,\omega)$ shown in Figs. 5(a) and 5(b) highlights the SOQ. At the SU(4) point [Fig. 5(a)] it appears as a δ function, $A_0(Q,\omega) = \delta\{\omega - \omega_{\mathrm{SOQ}}(Q)\}$, whereas in Fig. 5(b) the SOQ is damped and its intensity decreases strongly with Q. The decrease of peak heights is a consequence of the increasing line width $\Gamma(Q)$ of the SOQ for $Q \to 0$. In the latter figure the BS at the low energy side of the continuum appears as a weak additional feature, while it is absent in (a), i.e., at the SU(4) point. The nearest neighbor spectral functions, $A_{1+}(Q,\omega)$ in Fig. 5(c) and $A_{1-}(Q,\omega)$ in Fig. 5(d), show both the spin-orbital continuum and the BS below the continuum. Notably, comparing with the vNE spectral function in Fig. 3, we find the same characteristic energies and similar intensity features as in the RIXS spectra. The spectral function provides information of various correlations which could serve to derive the reduced density matrices.[57]

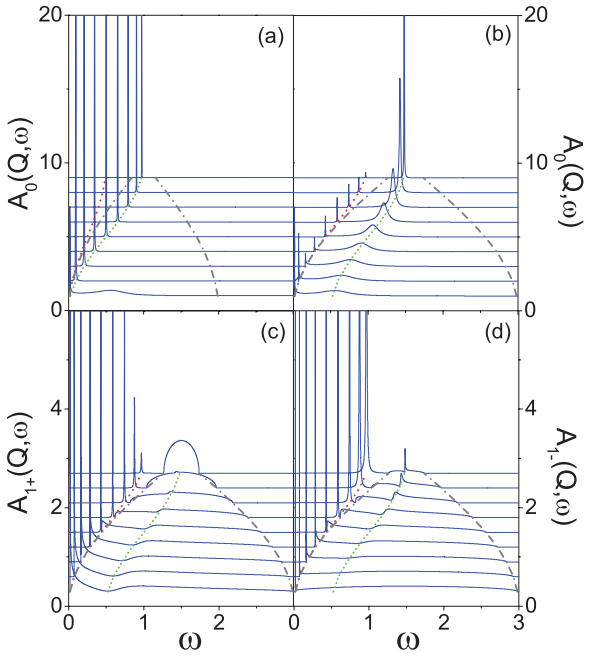

FIG. 5. (Color online) Upper part—the spectral function of the on-site excitation $A_0(Q,\omega)$ for: (a) $x = y = 1/4$, (b) $x = y = 1/2$. Lower part—the nearest-neighbor spectral functions for $x = y = 1/2$: (c) $A_{1+}(Q,\omega)$ and (d) $A_{1-}(Q,\omega)$. The momentum range in each panel from $\pi/10$ (bottom) to $9\pi/10$ (top); the peak broadening is $\eta = 0.01$. Dashed (red) and dotted (green) lines correspond to the BS and to the SOQ, while gray dash-dot lines indicate the boundaries of the continuum.

V. SUMMARY AND OUTLOOK

In this paper, we study a spin-orbital system and extend the analysis of entanglement to elementary excited states by introducing the vNE spectral function. The vNE is calculated from the reduced density matrix describing the spin sector of the individual energy eigenstate which is obtained after performing the trace over the orbital sector, or vice versa. Our study demonstrates that even in cases where the ground state of a spin-orbital chain is fully disentangled, e.g., in the ferro-ferro state, (i) the spin-orbital excitations are in general entangled, and (ii) maximal spin-orbital entanglement occurs for bound states which appear as sharp peaks in the vNE spectra.

Furthermore, we have shown that the vNE of undamped bound states exhibits a logarithmic dependence on the chain length L. At the SU(4) point the vNE of the spin-orbital quasiparticle excitations, which are eigenstates formed by Bloch states of local pairs of spin and orbital flips, emerge as sharp peaks of size $\log_2 L$ in the center of the spin-orbital excitation continuum with a dispersion $\omega_{\mathrm{SOQ}}(Q)$. Away from the SU(4) point the spin-orbital quasiparticle acquires finite quasiparticle lifetime and the spin-orbital correlations are controlled by a correlation length ξ, increasing with the distance from the SU(4) point. It turns out that the vNE of this state is controlled by the spin-orbital correlation length and decays logarithmically with ξ.

Guided by the close relationship of the vNE and the degree of spin-orbital correlations in the wave functions, we have addressed the question whether there is direct experimental

access to these correlations and therefore a way to explore the von Neumann spectral functions by some sort of spectroscopy. Here we propose to study the dynamic spin-orbital correlation functions as a qualitative measure of the vNE spectra, and suggest to use resonant inelastic x-ray scattering as a promising technique. We have shown that this method would allow us to highlight particular states via selection rules.

ACKNOWLEDGMENTS

We acknowledge insightful discussions with Maurits W. Haverkort and Krzysztof Wohlfeld. W.-L.Y. acknowledges support by the National Natural Science Foundation of China (NSFC) under Grant No. 11004144. A.M.O. acknowledges support by the Polish National Science Center (NCN) under Project No. N202 069639.

[1] Y. Tokura and N. Nagaosa, Science **288**, 462 (2000).

[2] J. Schlappa, K. Wohlfeld, K. J. Zhou, M. Mourigal, M. W. Haverkort, V. N. Strocov, L. Hozoi, C. Monney, S. Nishimoto, S. Singh, A. Revcolevschi, J.-S. Caux, L. Patthey, H. M. Rønnow, J. van den Brink, and T. Schmitt, Nature (London) **485**, 82 (2012).

[3] L. F. Feiner and A. M. Oleś, Phys. Rev. B **59**, 3295 (1999); N. N. Kovaleva, A. M. Oleś, A. M. Balbashov, A. Maljuk, D. N. Argyriou, G. Khaliullin, and B. Keimer, *ibid.* **81**, 235130 (2010).

[4] S. Krivenko, Phys. Rev. B **85**, 064406 (2012).

[5] G. Khaliullin and S. Maekawa, Phys. Rev. Lett. **85**, 3950 (2000).

[6] P. Horsch, A. M. Oleś, L. F. Feiner, and G. Khaliullin, Phys. Rev. Lett. **100**, 167205 (2008).

[7] K. Wohlfeld, M. Daghofer, and A. M. Oleś, Europhys. Lett. **96**, 27001 (2011).

[8] G. Jackeli and G. Khaliullin, Phys. Rev. Lett. **102**, 017205 (2009).

[9] W. Brzezicki and A. M. Oleś, Phys. Rev. B **83**, 214408 (2011); Acta Phys. Polon. A **121**, 1045 (2012), http://przyrbwn.icm.edu.pl/APP/ABSTR/121/a121-5-16.html.

[10] K. Wohlfeld, M. Daghofer, S. Nishimoto, G. Khaliullin, and J. van den Brink, Phys. Rev. Lett. **107**, 147201 (2011).

[11] A. M. Oleś, P. Horsch, L. F. Feiner, and G. Khaliullin, Phys. Rev. Lett. **96**, 147205 (2006).

[12] A. M. Oleś, J. Phys.: Condens. Matter **24**, 313201 (2012).

[13] Y. Tanaka, A. Q. R. Baron, Y-J. Kim, K. J. Thomas, J. P. Hill, Z. Honda, F. Iga, S. Tsutsui, D. Ishikawa, and C. S. Nelson, New J. Phys. **6**, 161 (2004).

[14] F. Forte, L. J. P. Ament, and J. van den Brink, Phys. Rev. Lett. **101**, 106406 (2008).

[15] C. Ulrich, L. J. P. Ament, G. Ghiringhelli, L. Braicovich, M. M. Sala, N. Pezzotta, T. Schmitt, G. Khaliullin, J. van den Brink, H. Roth, T. Lorenz, and B. Keimer, Phys. Rev. Lett. **103**, 107205 (2009).

[16] H. Shiba, R. Shiina, and A. Takahashi, J. Phys. Soc. Jpn. **66**, 941 (1997).

[17] R. Kilian and G. Khaliullin, Phys. Rev. B **58**, R11841 (1998).

[18] J. van den Brink, P. Horsch, F. Mack, and A. M. Oleś, Phys. Rev. B **59**, 6795 (1999).

[19] F. Mack and P. Horsch, Phys. Rev. Lett. **82**, 3160 (1999).

[20] J. van den Brink, P. Horsch, and A. M. Oleś, Phys. Rev. Lett. **85**, 5174 (2000); J. van den Brink, *ibid.* **87**, 217202 (2001).

[21] J. Bała and P. Horsch, Phys. Rev. B **72**, 012404 (2005).

[22] S. Ishihara, Phys. Rev. B **69**, 075118 (2004); Phys. Rev. Lett. **94**, 156408 (2005).

[23] J. Zaanen and A. M. Oleś, Phys. Rev. B **48**, 7197 (1993); A. Gorschlüter and H. Merz, *ibid.* **49**, 17293 (1994).

[24] J. van den Brink, W. Stekelenburg, D. I. Khomskii, G. A. Sawatzky, and K. I. Kugel, Phys. Rev. B **58**, 10276 (1998).

[25] C. Itoi, S. Qin, and I. Affleck, Phys. Rev. B **61**, 6747 (2000).

[26] J. Sirker and G. Khaliullin, Phys. Rev. B **67**, 100408 (2003).

[27] S. Miyashita and N. Kawakami, J. Phys. Soc. Jpn. **74**, 758 (2005).

[28] L. F. Feiner, A. M. Oleś, and J. Zaanen, Phys. Rev. Lett. **78**, 2799 (1997); J. Phys.: Condens. Matter **10**, L555 (1998).

[29] J. Bała, A. M. Oleś, and G. A. Sawatzky, Phys. Rev. B **63**, 134410 (2001).

[30] A. Herzog, P. Horsch, A. M. Oleś, and J. Sirker, Phys. Rev. B **83**, 245130 (2011).

[31] G. Sun, G. Jackeli, L. Santos, and T. Vekua, arXiv:1112.5082 (unpublished).

[32] Y.-Q. Li, M. Ma, D.-N. Shi, and F.-C. Zhang, Phys. Rev. B **60**, 12781 (1999).

[33] B. Sutherland, Phys. Rev. B **12**, 3795 (1975).

[34] V. Alba, M. Fagotti, and P. Calabrese, J. Stat. Mech. (2009) P10020.

[35] H. Li and F. D. M. Haldane, Phys. Rev. Lett. **101**, 010504 (2008).

[36] H. Yao and X.-L. Qi, Phys. Rev. Lett. **105**, 080501 (2010).

[37] A. Kitaev and J. Preskill, Phys. Rev. Lett. **96**, 110404 (2006).

[38] I. Klich and L. Levitov, Phys. Rev. Lett. **102**, 100502 (2009).

[39] J. Eisert, M. Cramer, and M. B. Plenio, Rev. Mod. Phys. **82**, 277 (2010).

[40] L. Bombelli, R. K. Koul, J. Lee, and R. D. Sorkin, Phys. Rev. D **34**, 373 (1986); M. Srednicki, Phys. Rev. Lett. **71**, 666 (1993); S. W. Hawking, J. Maldacena, and A. Strominger, J. High Energy Phys. 05 (2001) 001.

[41] L. Amico, R. Fazio, A. Osterloh, and V. Vedral, Rev. Mod. Phys. **80**, 517 (2008).

[42] C. Holzhey, F. Larsen, and F. Wilczek, Nucl. Phys. B **424**, 443 (1994).

[43] L. Masanes, Phys. Rev. A **80**, 052104 (2009).

[44] J. Sirker, A. Herzog, A. M. Oleś, and P. Horsch, Phys. Rev. Lett. **101**, 157204 (2008).

[45] Y. Chen, Z. D. Wang, Y. Q. Li, and F. C. Zhang, Phys. Rev. B **75**, 195113 (2007).

[46] S.-J. Gu, Int. J. Mod. Phys. B **24**, 4371 (2010).

[47] W.-L. You, Y.-W. Li, and S.-J. Gu, Phys. Rev. E **76**, 022101 (2007).

[48] M. Wortis, Phys. Rev. **132**, 85 (1963).

[49] T. Schneider, Phys. Rev. B **24**, 5327 (1981).

[50] S. Cojocaru and A. Ceulemans, Phys. Rev. B **67**, 224413 (2003).

[51] D. P. Arovas and A. Auerbach, Phys. Rev. B **52**, 10114 (1995).

[52] Dyson equation reads $G^{-1}(Q,\omega) = \omega - \omega_{\mathrm{SOQ}}(Q) - \Sigma(Q,\omega)$, with the total self-energy $\Sigma(Q,\omega)$. The real part $\mathrm{Re}G^{-1}(Q,\omega)$ identifies the effective energy pole, and the imaginary part of self-energy is the inverse of lifetime τ, i.e., $\Gamma = \mathrm{Im}\Sigma(Q,\omega)$.

[53] L. Cincio, J. Dziarmaga, M. M. Rams, and W. H. Zurek, Phys. Rev. A **75**, 052321 (2007).

[54] S. Ishihara and S. Maekawa, Phys. Rev. B **62**, 2338 (2000).

[55] M. W. Haverkort, Phys. Rev. Lett. **105**, 167404 (2010).

[56] L. J. P. Ament, M. van Veenendaal, T. P. Devereaux, J. P. Hill, and J. van den Brink, Rev. Mod. Phys. **83**, 705 (2011).

[57] I. Peschel and V. Eisler, J. Phys. A: Math. Theor. **42**, 504003 (2009).